Supplemental Document

Biomedical Optics EXPRESS

Two-photon peak molecular brightness spectra reveal long-wavelength enhancements of multiplexed imaging depth and photostability: supplement

RYAN T. LANG[1,2] AND BRYAN Q. SPRING[1,2,3,*]

[1] *Translational Biophotonics Cluster, Northeastern University, Boston, MA 02115, USA*
[2] *Department of Physics, Northeastern University, Boston, MA 02115, USA*
[3] *Department of Bioengineering, Northeastern University, Boston, MA 02115, USA*
[*] *b.spring@northeastern.edu*

Supplement DOI: https://doi.org/10.6084/m9.figshare.16437033

Parent Article DOI: https://doi.org/10.1364/BOE.433989

Two-photon peak molecular brightness spectra evince long-wavelength enhancements of multiplexed imaging depth and photostability: supplemental document

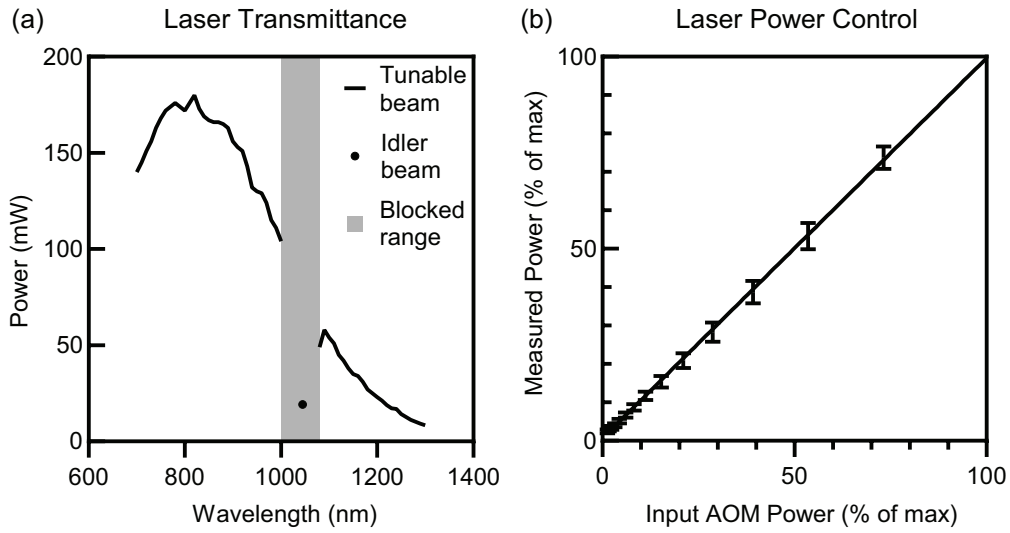

Fig. S1. (a) Laser power delivered at the objective *vs* wavelength for the setup described in Section 2.1. Measurement recorded in 10 nm steps at 100% laser power output. (b) Correlation of measured laser power *vs* input percent specified by user. Individual values measured at wavelengths between 700 and 1300 nm in steps of 100 nm; data are mean ± SD.

Dye	A488	A514	A546	A568	A594	A610	A633
pH (±0.1)	6.1	6.2	6.1	6.2	6.1	5.9	6.0

Table S1. Measurements of pH values of dilute dye solutions described in Section 2.1 of Alexa Fluor probes at 1-10 nM in DI H_2O. All values are well within the stable range specified by ThermoFisher (pH 4-10).

Dye	A488	A514	A546	A568	A594	A610	A633
ρ	0.944	0.953	0.990	0.990	0.988	0.993	0.990

Table S2. Pearson coefficients of correlation ρ for sections of peak molecular brightness curves also presented in Mütze *et al.*, Biophys. J, 2012 [3]. All repeated measurements show high correlation ($P < 0.0001$ for all values), demonstrating repeatability of peak molecular brightness across different experimental setups.

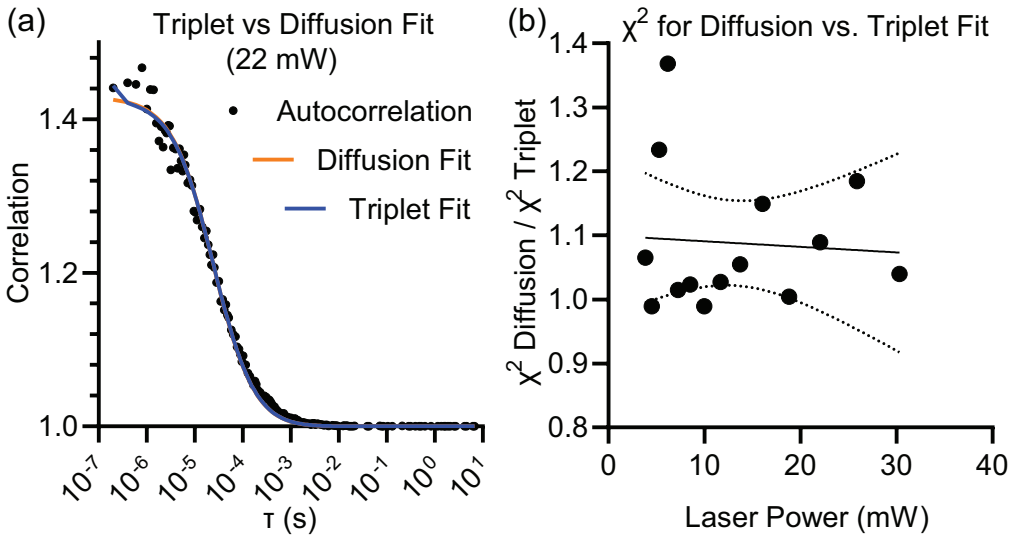

Fig. S2. (a) Simple diffusion and triplet fit for A532 at 22 mW, 790 nm shows no significant improvement to the fit by including the triplet term. (b) Reduced chi-squared ratio for diffusion versus triplet fits for A532 at 790 nm across powers. True triplet dynamics would increase significantly at higher powers; here reduced chi-squares for triplet fits are only improved overall since it has 5 degrees of freedom instead of 3. The slope is negative (expected to be positive if triplet fit is better at high powers), but not significantly different than 0 ($P = 0.82$, F-test). Triplet fits were the same as the diffusion fit (Eq. 1) multiplied by additional term $[1 - T + T * exp(-\tau/\tau_t)$, where $T]$ is the triplet population fraction and τ_t the triplet lifetime, as shown by Dittrich *et al.*[4]

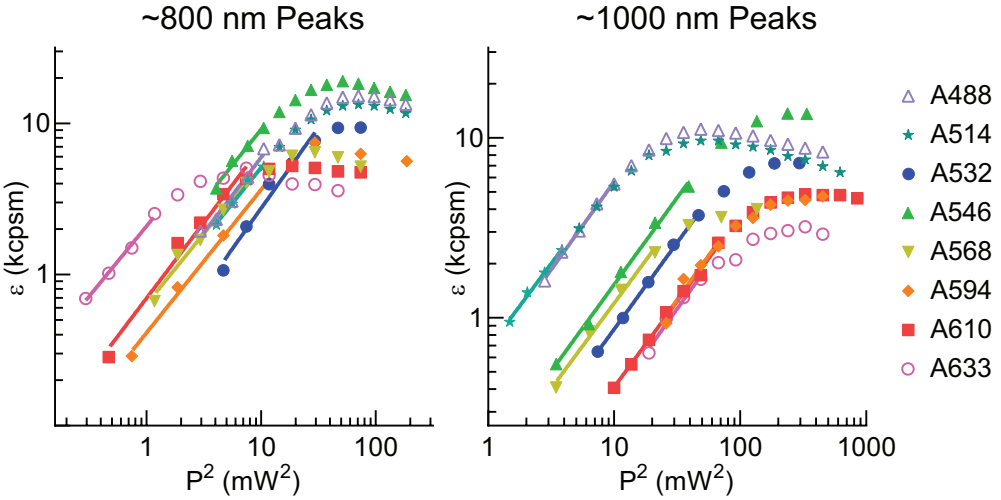

Fig. S3. Power spectra for ∼800 nm and ∼1000 nm peaks described in Section 3.1. All peaks exhibit a power-squared dependence on signal for low laser power, which deteriorates as bleaching and saturation effects dominate the relationship at high laser power. Best fit lines are included for the domain where the power-squared law dominates.

	~800 nm Peak			~1000 nm Peak		
Dye	λ (nm)	ε_{max} (kcpsm)	P^2 vs. ε slope	λ (nm)	ε_{max} (kcpsm)	P^2 vs. ε slope
A488	760	15.671	0.99 ± 0.09	910	11.156	0.98 ± 0.04
A514	770	13.285	0.95 ± 0.06	940	9.627	0.94 ± 0.06
A532	770	12.559	1.07 ± 0.10	970	8.720	0.96 ± 0.02
A546	820	18.987	0.94 ± 0.09	1100	13.631	0.96 ± 0.04
A568	790	6.733	0.93 ± 0.08	1080	4.024	0.95 ± 0.07
A594	810	8.725	0.95 ± 0.05	1080	6.161	0.98 ± 0.19
A610	830	6.950	1.00 ± 0.08	1100	7.095	0.95 ± 0.03
A633	830	5.174	0.93 ± 0.05	1120	3.593	0.98 ± 0.10

Table S3. Additional data for peaks shown in Fig. 2 and Fig. S3. Peak wavelength (λ) and height (ε_{max}) are shown, as well slopes for best fit lines of power squared *vs* ε plots. Two-photon fluorescence is expected to produce a slope of 1.0 on this plot. Slopes are presented as mean $\pm$ SEM.

	790 nm excitation		1090 nm excitation	
Dye	$A = \varepsilon / P^2$ fit	$\sqrt{\varepsilon_{max} / A\lambda^2}$ (norm)	$A = \varepsilon / P^2$ fit	$\sqrt{\varepsilon_{max} / A\lambda^2}$ (norm)
A532	0.05036	0.226	0.00185	1.000
A546	0.10700	0.201	0.01234	0.741
A568	0.24930	0.091	0.01831	0.391
A594	0.08364	0.143	0.02335	0.367
A610	0.10190	0.117	0.03128	0.363
A633	0.08528	0.097	0.01375	0.368

Table S4. Data used for calculating predicted bleaching half-life from molecular brightness measurements. The fit from the power spectrum $A = \varepsilon / P^2$ (units of kcpsm/mW^2) is shown as well as the prediction of relative half-life, $\sqrt{\varepsilon_{max} / A\lambda^2}$, which is normalized to the highest value (A532 at 1090 nm)

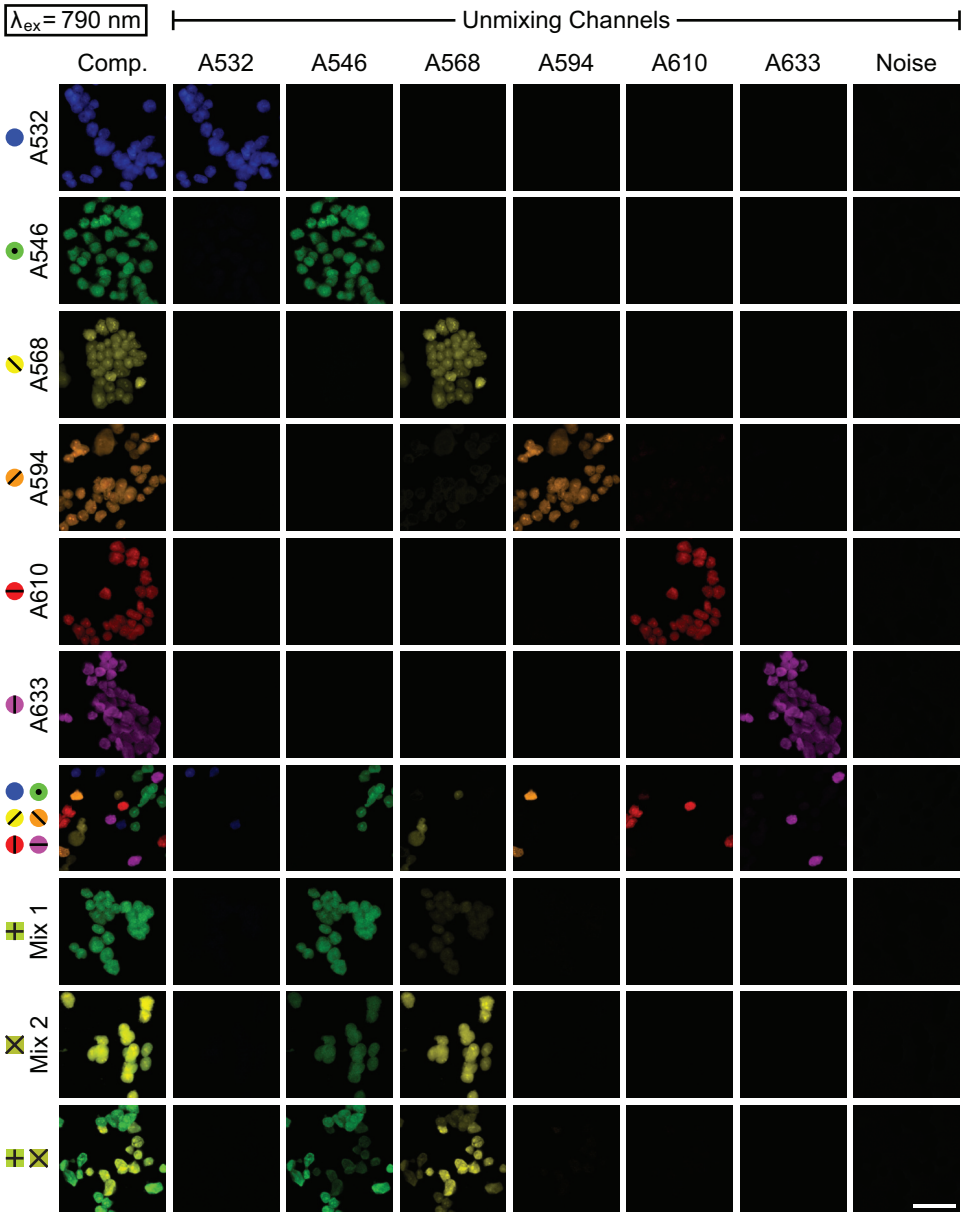

Fig. S4. Unmixing breakout panel of slides of stained cells imaged with the setup described in Section 2.2 at λ_{ex} = 790 nm. Ten rows show the variants of stained cells used in both tissue phantoms. Six single-dye cell types are shown (rows 1-6) as well as all six on a single slide (row 7). Two mix-dye variants (rows 8-9) and both on a single slide (row 10) are also shown. Scale bar is 50 μm.

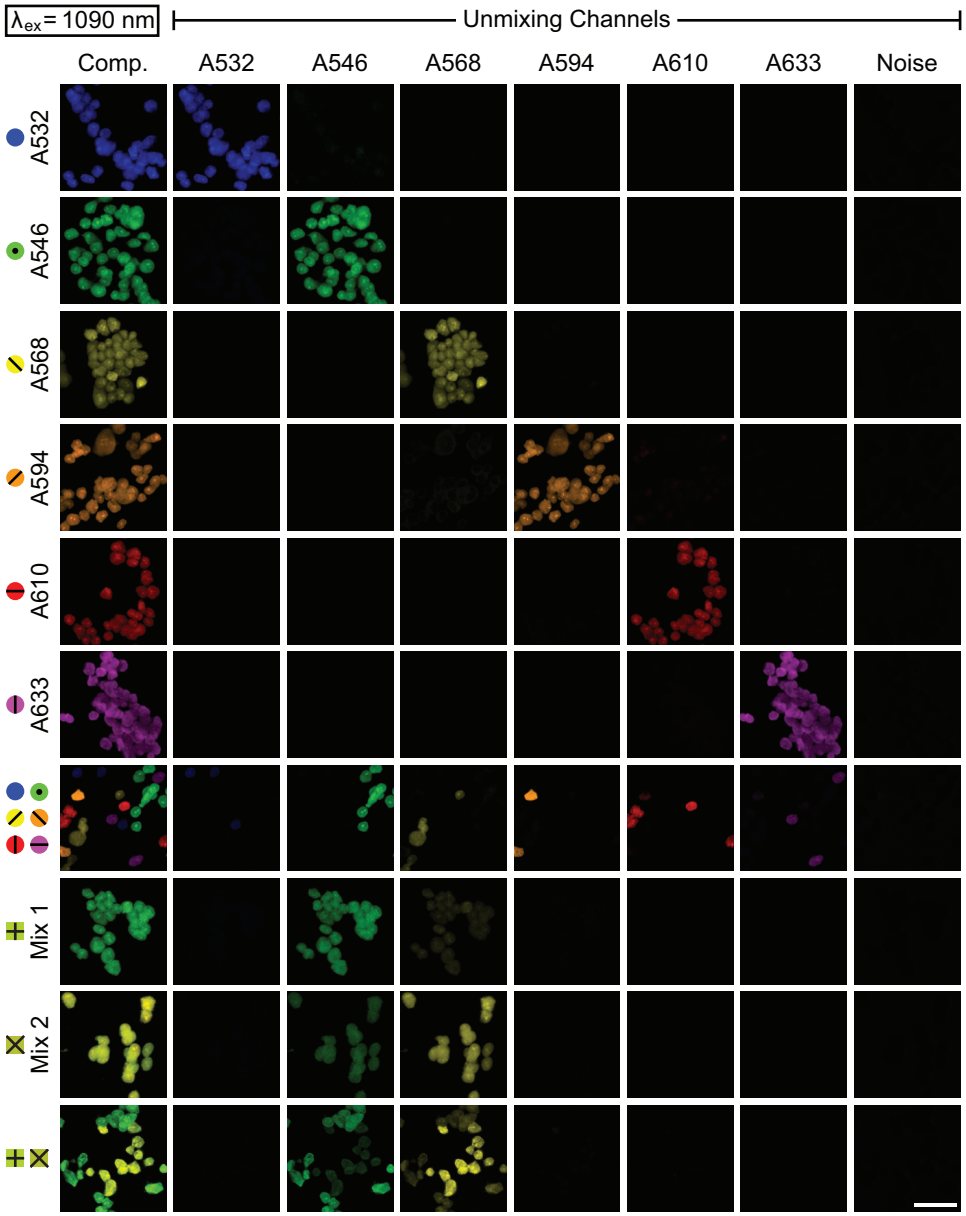

Fig. S5. Unmixing breakout panel of slides of stained cells imaged with the setup described in Section 2.2 at λ_{ex} = 1090 nm. Ten rows show the variants of stained cells used in both tissue phantoms. Six single-dye cell types are shown (rows 1-6) as well as all six on a single slide (row 7). Two mix-dye variants (rows 8-9) and both on a single slide (row 10) are also shown. Scale bar is 50 μm.

SUPPLEMENTARY METHODS

A. Two-Photon FCS with a Commercial Microscope

Two photon peak molecular brightness spectra were measured by adapting a commercial microscope to perform FCS experiments on dilute fluorophore samples. The LSM 880 microscope was installed with nonlinear excitation capabilities: the horizontally polarized output of a tunable, mode-locked, femtosecond-pulse laser (InSight®X3™ DUAL-AX; SpectraPhysics) was coupled into an acousto-optic modulator (000000-2103-400, Zeiss) to control output laser power. Group-delay dispersion (GDD) was controlled automatically by the DeepSee dispersion precompensation module integrated in the InSight X3 laser, which optimizes compensation as part of mode-locking (*i.e.* at every wavelength). The beam was then coupled and aligned into a laser input port on the LSM 880. The microscope's internal components directed the beam to fill the back aperture of a 40x, 1.2 NA water-immersion objective (C-Apochromat 40x/1.20 W Corr M27; 421767-9973-799, Zeiss) which focused the beam through a #1.5 coverslip into the dye sample, held in a sample dish (P50G-1.5-14-F, Mattek).

Fluorescence was collected with the same objective and passed through a dichroic mirror (BS MP UV/690+; 447962-9001-000, Zeiss) before being detected by the 32 channel "Quasar" GaAsP PMT (000000-2179-906, Zeiss) in the LSM 880. The PMT was operated in photon counting mode, where all photon counts from active channels are summed. The focal volume was consistently placed 200 μm below the cover slip to maintain a consistent focal volume across all dyes. Care was taken so that the total time-averaged fluorescence signal $\langle F(t)\rangle$ never exceeded 500 kilocounts per second to avoid detector saturation. Additionally, all measurements were taken with all room lights, computer monitors and other light sources turned off to avoid detection of any non-fluorescent photons. Data collection was automated by an AutoHotkey script that operated the controls and curve fitting of the ZEN software and saved the laser wavelength, laser power, fitted fluorescence correlation amplitude $G(0)$, and fluorescence intensity $\langle F(t)\rangle$, for each FCS measurement.

The fluorescence signal has been shown to be improved if solutions are prepared in DI H_2O instead of typical pH-buffered solutions, presumably due to some mild quenching effects from the buffers. In order to maximize signal to noise, all solutions were prepared in DI H_2O. This has the potentially adverse effect of destabilizing the pH; DI H_2O is typically mildly acidic due to dissolved atmospheric CO_2. While this effect may cause instability of signal levels for other fluorophores, the Alexa Fluor dyes are stable between pH 4-10 (Manufacturer's guidelines), which the measured values (Supplementary Table S1) are well within.

The Alexa Fluor dyes are well characterized in the literature, with chemical structures and other spectroscopic properties freely and publicly available. For example, structures can be found at https://www.atdbio.com/content/34/Alexa-dyes, or in Panchuck-Voloshina *et al.* (https://doi.org/10.1177/002215549904700910)[1], or in selected chapters of the Handbook of Fluorescent Dyes and Probes by R. W. Sabnis (https://doi.org/10.1002/9781119007104)[2].

B. Physical Properties of Molecular Brightness Measurements

Relation of Molecular Brightness and TPA Cross-Section

The molecular brightness $\varepsilon = \langle F(t)\rangle / N_{AC}$ can be directly related to the TPE action cross section $\sigma_2\eta_2$ in the absence of ground state depletion or bleaching effects. Following Mütze *et al.* [3], the time-averaged fluorescence signal $\langle F(t)\rangle$ depends on the TPA cross-section σ_2, the quantum yield η_2, and the incident photon flux through the excitation volume. For a mode-locked, pulsed laser, the photon flux can be written as a function of average intensity $I_{ave} = \langle I_0(t)\rangle$, photon energy hc/λ, and the second order temporal coherence $g = \langle I_0^2(t)\rangle / \langle I_0(t)\rangle^2$. The calculation of g is standardized by writing $g = g_p f\tau$, where $f\tau$ is the duty cycle (the pulse repetition rate f multiplied by the temporal full width half maximum τ), and the dimensionless quantity g_p has been published for common temporal pulse shapes [5]. The incident photon flux is then $[g_p/(f\tau)] * [I_{ave}/(hc/\lambda)]^2$, and the molecular brightness follows as

$$\varepsilon = \frac{1}{2}\sigma_2\eta_2 \frac{g_p\phi}{f\tau} \frac{I_{ave}^2}{(hc/\lambda)^2}\gamma. \tag{S1}$$

where ϕ is the overall collection efficiency. The quantity γ is the "volume contrast" which functionally depends on the shape of the point spread function and is published for typical theoretical point spread functions [3]. Since two incident photons are required to produce one fluorescence photon, a factor of $1/2$ is included.

This formula can be re-written to allow calculation of the TPE action cross section from molecular brightness measurements as:

$$\sigma_2\eta_2 = \left[\frac{\varepsilon}{P_{ave}^2}\right]\frac{f\tau}{g_p\phi\gamma}\frac{\omega_0^4\pi^2}{2}\left(\frac{hc}{\lambda}\right)^2. \tag{S2}$$

where the intensity has been expressed in terms of the average power and the beam waist ω_0 as $I_{ave} = 2P_{ave}/\omega_0^2\pi$. Here, the bracketed term ε/P_{ave}^2 can be calculated by fitting molecular brightness versus power squared. However, determination of a robust fit is not always possible, especially for troughs in the spectrum where even peak molecular brightness signal is low. For these cases, there can be insufficient signal at low power to determine this fit.

In the present study, thermal heating of the solvent and electronic nonlinearity of the solvent were not included. We expect the magnitude of these effects to be marginal for the given power levels, peak intensities, and exposure times used.

Physical Meaning of Peak Molecular Brightness

The peak molecular brightness arises from an intersection of several competing photophysical processes. As discussed by Iyer and colleagues, the molecular brightness deviates from the power squared dependence due to photobleaching and volume saturation effects [6]. The peak molecular brightness ε_{max} results from nonlinear photobleaching overpowering the benefit on fluorescence of increasing laser intensity. Iyer showed that the peak value is reached before the regime where saturation effects are dominant (very high powers), and that while a functional form is not known, ε_{max} is dependent on η_2 and η_b, the two-photon fluorescence and bleaching quantum efficiencies, respectively.

Mütze *et al.* showed further that the dominant photobleaching mechanism was highly nonlinear (greater than quadratic dependence) [3]. Due to this result, η_b is spectrally anti-correlated to with σ_2, since bleaching increases more rapidly than absorption with intensity. This implies ε_{max} should be correlated with $\eta_2\sigma_2$, which was found to be true. Finally, the physical meaning of ε_{max} can be interpreted as an integrative measurement of both fluorescence cross-section and photostability. Large peak brightness results from a combination of high photostability and cross section.

The two-photon action cross section informs the efficiency of fluorescence per potential absorption event. Alternatively, the peak molecular brightness is the maximum molecular fluorescence intensity per molecule, for a given laser and detection setup. As argued by Iyer *et al.*, the cross-section measurement is typically favored by the community since it is the most relevant parameter for imaging with low power to limit specimen heating. However, ε_{max} is the more relevant metric for predict signal quality when the average power is not the limiting factor. In these scenarios, it is important to consider the photostability of the fluorophores as well as the fluorescence yield for experimental design.

C. Prediction of Relative Bleaching Half-Life

As reported in Mütze *et al.* [3], the parameter $\varepsilon_{max}/\sigma_2\eta_2$ has been shown to predict photostability. While direct calculation of $\sigma_2\eta_2$ is arduous (Eq. S2), normalization of $\varepsilon_{max}/\sigma_2\eta_2$ to a maximum value allows most of the formula to fall out as constants. By normalizing, only wavelength-dependent terms remain:

$$\frac{\varepsilon_{max}/\sigma_2\eta_2}{[\varepsilon_{max}/\sigma_2\eta_2]_{max}} = \frac{\varepsilon_{max}/A\lambda^2}{[\varepsilon_{max}/A\lambda^2]_{max}} \tag{S3}$$

where $A = \varepsilon/P_{ave}^2$ is the fit parameter from the power spectrum. Here, all other terms in Eq. S2 have been assumed to be independent of laser excitation wavelength, except for ω_0 which is known to be proportional to the wavelength [7]. The wavelength independence is a reasonable first-order approximation for the Insight X3 as f and τ are expected to not change more than 5% for the wavelengths examined here (manufacturers specifications); the temporal coherence g_p, volume contrast γ and collection efficiency ϕ are not expected to have any excitation wavelength dependence for a single dye (*e.g.*, the emission spectrum is independent of excitation wavelength). Changes in collection efficiency due to different emission wavelengths among the dyes could affect the measured photon counts, but these should change both ε_{max} and ε by the same amount, so this variation is expected to be marginal.

To enable linear comparison to the photobleaching half-life, the square root of $\varepsilon_{max}/\sigma_2\eta_2$ was taken. Motivation can be demonstrated from a dimensional analysis of $\varepsilon_{max}/\sigma_2\eta_2$ and

the half-life. The photobleaching half-life reports the number of frames of sequential imaging needed to decrease the signal by 50%. The unit of a frame can be understood as a number of excitation photons per area and time from the fluorophores perspective. That is, a frame can be thought to have units of photons/m^2s. The units of $\varepsilon_{max}/\sigma_2\eta_2$ are photons^2/m^4s^2, as ε_{max} has units of photons per second per molecule, and $\sigma_2\eta_2$ has units of Goeppert-Mayers. Therefore, $\sqrt{\varepsilon_{max}/\sigma_2\eta_2}$ has units of photons/m^2s and is more appropriate for linear comparison (*i.e.* Pearson's correlation) to the photobleaching half-life. The final values reported as the predicted relative half-life are found by taking the square root of the right hand side of Eq. S3.

D. Calculation of Unmixing Error to Signal Ratio

The unmixing error to signal ratio was created to enable a measurement of the integrity of unmixing results on a per-pixel basis. A given pixel x consists of a vector of relative abundances of the unmixing components (*i.e.* fluorophores). These are compared to the possible ground truths c_i corresponding to the cell staining procedure. For the single-dye panel, c_i are the rows of the identity matrix, as only one basis member is expected at each pixel. For the mixed-dye panel, c_i are the two relative abundances as measured in the control slides. That is, each i corresponds to a type of cell stain.

The unmixing error is calculated as $\delta = \Sigma(x - c_i)$, where the index i is selected such that $x - c_i$ is minimized. That is, the error is reported as the sum of the differences between the pixel and the closest matching ground truth. The pixel x and ground truth c_i are normalized so the maximum value is 1. Therefore, the signal level (level of the brightest endmember) is always set to 1 and the unmixing error to signal ratio is equal to δ. With this normalization, δ is the sum of error (signal in the wrong dye channels) relative to the signal level.

Images were pre-processed by autothresholding using Otsu's method, to only consider images containing contrast agents. Additionally, only pixels belonging to contiguous regions of 30 or more pixels were considered (implemented using MATLAB's regionprops function).

REFERENCES

1. N. Panchuk-Voloshina et al. "Alexa Dyes, a Series of New Fluorescent Dyes that Yield Exceptionally Bright, Photostable Conjugates." J. Histochem. Cytochem. **47**, 1179–1188 (1999).
2. R. W. Sabnis, *Alexa Fluor Dyes* (John Wiley & Sons, Ltd, 2015), chap. 7-12, pp. 20–34.
3. Mütze, J. et al. "Excitation spectra and brightness optimization of two-photon excited probes." Biophys. J. **102**, 934–944 (2012).
4. Dittrich P. & Schwille, P. S., "Photobleaching and stabilization of fluorophores used for single-molecule analysis withone-and two-photon excitation." Appl. Phys. **B73**, 829–837 (2001).
5. Xu, C. & Webb, W. W. "Measurement of two-photon excitation cross sections of molecular fluorophores with data from 690 to 1050 nm." J. Opt. Soc. Am. B 13, 481 (1996).
6. Iyer, V., Rossow, M. J. & Waxham, M. N. "Peak two-photon molecular brightness of fluorophores is a robust measure of quantum efficiency and photostability." J. Opt. Soc. Am. B 23, 1420 (2006).
7. Zipfel, W. R., Williams, R. M. & Webb, W. W. "Nonlinear magic: Multiphoton microscopy in the biosciences." Nat. Biotechnol. 21, 1369–1377 (2003).